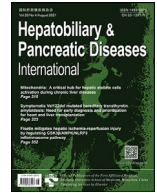




Contents lists available at ScienceDirect

## Hepatobiliary &amp; Pancreatic Diseases International

journal homepage: [www.elsevier.com/locate/hbpd](http://www.elsevier.com/locate/hbpd)

## New Techniques

## Raman spectroscopy in the diagnosis of malignant biliary stricture: A feasibility study

Peter Slodička<sup>a,b</sup>, Přemysl Falt<sup>a,b</sup>, Václav Ranc<sup>c,\*</sup>, Vincent Dansou Zoundjiekpon<sup>a,b</sup>, Ondřej Urban<sup>a,b</sup><sup>a</sup>2nd Department of Internal Medicine - Gastroenterology and Geriatrics, University Hospital Olomouc, Olomouc, Czech Republic<sup>b</sup>Faculty of Medicine and Dentistry, Palacky University, Olomouc, Czech Republic<sup>c</sup>Institute of Molecular and Translational Medicine, Faculty of Medicine, Palacky University, Olomouc, Czech Republic

Biliary strictures are caused by both benign and malignant pathologies. Although up to 30% of biliary strictures are identified as benign, the vast majority are malignant with two major malignancies, namely pancreatic adenocarcinoma and cholangiocarcinoma (CC) [1]. Accurate diagnosis and precise localization play a vital role in the prognosis and management of the disease [2].

In this study we primarily focused on the diagnosis of CC. The highest incidence of CC is in northeastern Thailand, where the incidence is found to be 100/100 000 in males and 50/100 000 in females. In Western countries, it is approximately (0.5–2.0)/100 000 individuals [3]. CC is most often diagnosed between the ages of 70 and 80 years [4]. The prognosis of biliary malignancies is dismal with overall five-year survival as low as 10% [5].

CC is currently classified into two types according to its anatomic location along the biliary tree: intrahepatic (5%–10%) and extrahepatic CC [6]. The majority (60%–70%) of extrahepatic CC are perihilar or “Klatskin” tumors involving the bile duct confluence and are located above the cystic duct insertion [4,7].

Diagnosing CC at an early stage remains a challenge due to its asymptomatic feature, difficult to access anatomical location and highly desmoplastic, paucicellular nature of CC, which limit the sensitivity of cytological and histological diagnostic approaches [5,8,9]. CC generally presents with signs and symptoms of weight loss, pruritus and cholestasis [10]. Transabdominal ultrasonography has proven to be useful in detecting biliary tract dilation, severity of obstruction and the presence of gallstones. The direct visualization of CC on ultrasonography is usually impossible [5]. Computed tomography (CT) is an important diagnostic element in CC. The benefit of CT scanning for perihilar CC was evaluated in an analysis of 16 studies showing an accuracy of 86% for the ductal extent of CC [11]. The diagnostic performance of magnetic resonance imaging (MRI) is comparable to CT, while positron emission tomography/computed tomography (PET/CT) is the most beneficial for the detection of lymph nodes and metastases [12]. Endoscopic ultrasound (EUS) can be useful in the assessment of regional lymph nodes and as a method of biopsy for a suspicious primary

lesion [4]. However, in cases of proximal CC, due to increased risk of tumor seeding, EUS-guided biopsy of the primary lesion is contraindicated in liver transplant candidates [13]. Endoscopic retrograde cholangiopancreatography (ERCP) is a useful approach that has tissue access via brush cytology and/or biopsy [5,13]. Moreover, ERCP in many cases offers therapeutic relief of obstructing masses via stent placement [13]. The low sensitivity of bile duct brush cytology (commonly 20%–55%) presents a considerable diagnostic issue [14]. The fluorescence in situ hybridization (FISH) examination can in some cases increase sensitivity up to 50%–70%, while maintaining specificity, if combined with conventional brush cytology [14–16]. When imaging methods and biopsy fail to diagnose suspected malignant biliary stricture, cholangioscopy with forceps biopsy is recommended [17]. Nevertheless, cholangioscopy is expert-dependent, costly and not universally available [17].

None of the existing approaches allows real-time diagnosis with an adequate level of specificity and sensitivity. Due to the silent clinical course, two-thirds of CCs are diagnosed at an inoperable stage. Patient survival without treatment is only 3.9 months on average, and the survival of 12–15 months can be achieved with the use of palliative chemotherapy [18]. There is therefore a demand for a new approach that solely relies on an objective measurement of relevant tissue and bypasses limits of traditional tissue sampling. Raman spectroscopy is a potential platform that aims to satisfy these criteria [19]. Raman spectroscopy is a vibrational technique that examines biomolecular tissue structures, which has been shown to be beneficial in the detection of precancerous and cancerous lesions in various organs [20–22]. Raman spectroscopy has proven its potential to help endoscopists identify high risk pathological lesions as well as reduce the need for routine biopsies [23]. The biochemical and molecular tissue composition of pre-malignant (intestinal metaplasia, low grade dysplasia - LGD, high grade dysplasia - HGD) and malignant tissue of the oesophagus, stomach, colon, bladder and lung enable it to be differentiated from normal tissue after Raman spectroscopy is applied [20,22–30].

We developed a new method that can provide real-time Raman measurements of biliary stricture and physiological bile duct tissue during an ERCP procedure. The method is based on the uti-

\* Corresponding author.

E-mail address: [vaclav.ranc@upol.cz](mailto:vaclav.ranc@upol.cz) (V. Ranc).



**Fig. 1.** A fiber Raman probe starting from the end of the duodenoscope was introduced transpapillarily into the biliary stricture using an 8.5 Fr metal sheath during endoscopic retrograde cholangiopancreatography (ERCP). We can see the Raman probe right in the middle of the malignant biliary stricture.

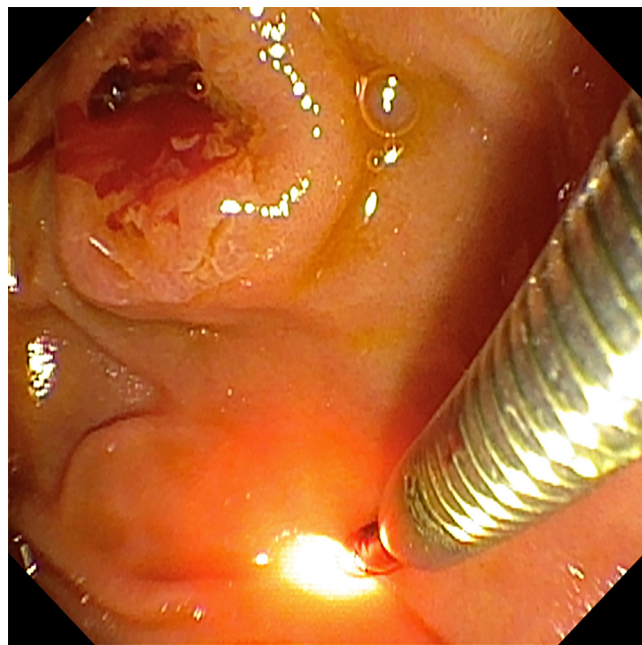


**Fig. 2.** Raman spectroscopy measurement in the duodenum under visual control. We see a Raman probe coming out of the metal sheath, and the red to white light around the probe was the light produced by the laser. Directly above the probe was the ampulla of Vater.

lization of a portable Raman system equipped with a fiber-optic probe. Then the resulting raw data are subjected to spectral processing and statistical evaluation, including a cluster analysis.

This study was conducted in a high-volume endoscopy center. It was approved by the Ethics Committee of the University Hospital and Faculty of Medicine of the Palacky University. All patients signed an informed consent. The inclusion criteria included subjects being over 18 years of age with suspected CC and indication for ERCP with sphincterotomy.

The Raman endoscopy instrumentation comprises a spectrum stabilized 785 nm diode laser (1804B000-FATBOY, Innovative Photonic Solutions, Plainsboro, USA), a transmissive imaging spectrograph (HT3-SPEC-785-CO2-F02-AN, EmVision advanced optical designs, Loxahatchee, USA), a near-infrared optimized, back-illuminated deep depletion charge-coupled device camera (Andor Newton EMCCD) and a specially designed Raman endoscopic probe for both laser light delivery and tissue Raman signal collection. Spectral resolution is given by grating, approximately  $8 \text{ cm}^{-1}$ .

The 1.65 mm diameter fiber-optic Raman endoscopic probe, which can fit into the instrument channel of medical endoscopes consists of 200-micron core fiber for Raman laser delivery and 200-micron core Raman collection fibers. The numerical aperture of these fibers is 0.22.

During ERCP, a fiber Raman probe was introduced transpapillarily into the biliary stricture using an 8.5 Fr metal sheath (Fig. 1). The Raman probe was placed in an adequate position under fluoroscopy control. The actual measurement was subsequently carried out (without fluoroscopy). All patients underwent sphincterotomy indicated for other reasons. The Raman spectroscopy of biliary stricture was performed 10–20 times (laser wavelength 785 nm, duration of each measurement 0.15 s). Tissues were always measured before the brush and never with the stent in place. The contrast fluid was present in the bile duct as well as in the duodenum during measurement. Measurements in the duodenum were performed under endoscopy control in the second part of duodenum (D2, 10–20 times) (Fig. 2). We did not turn off the white light from the endoscope when measuring in the duodenum. Immediately

after Raman acquisitions, the brush cytology was done to assess the etiology of the biliary stricture. The attained data were saved and processed by Andor Solis for Spectroscopy software (Andor, Belfast, UK). Raman spectra obtained from patients with a final diagnosis of CC were subsequently analyzed in collaboration with a biophysicist from the Institute of Molecular and Translational Medicine in Olomouc.

In total, we measured 20 patients with a mean age of 71 years (range 38–89); 45% of patients were males. A total of 815 measurements were performed, of which 466 (171 of CC, 154 of physiological bile duct, 141 of duodenal tissue) were subsequently analyzed. We performed 10–20 Raman measurements of tissue indicated as suspected CC (based on the fluoroscopy image during ERCP), healthy tissue and duodenal mucosa for each of the selected 20 patients where biliary stricture indicated ERCP with sphincterotomy. Diagnoses based on brush cytology findings were in most cases: extrahepatic CC ( $n = 11$ ); proximal CC,  $n = 10$ ; distal  $n = 1$ ), ampullary tumor ( $n = 6$ ); adenocarcinoma,  $n = 3$ ; adenoma HGD,  $n = 2$ ; adenoma LGD,  $n = 1$ ) and primary sclerosing cholangitis ( $n = 1$ ). Two patients finally had physiological findings on the biliary tract, without biliary stricture. Since the most common final diagnosis of biliary stricture among enrolled patients was CC, we decided to only evaluate whether there were differences in the measured Raman spectra between CC and physiological biliary tissue. We did not have enough data to evaluate whether there are differences between CC/physiological bile tissue and other types of biliary strictures. It is noteworthy that transpapillary insertion of the probe was not successful in 5 cases. The procedures were always only performed by an experienced endoscopist. No procedure related complications were noted in any of the patients. No mechanical damage to the probes was observed. No damaged tissue was observed when the pathology was reported.

Raman spectra were pre-processed and evaluated in the R environment for statistical computing, in particular using R package ChemoSpec (Hanson B. Package Version 2.0–2). First, the spectral region from  $700\text{--}1800 \text{ cm}^{-1}$  was selected for further analysis to remove silent regions and redundant data. The selected region in

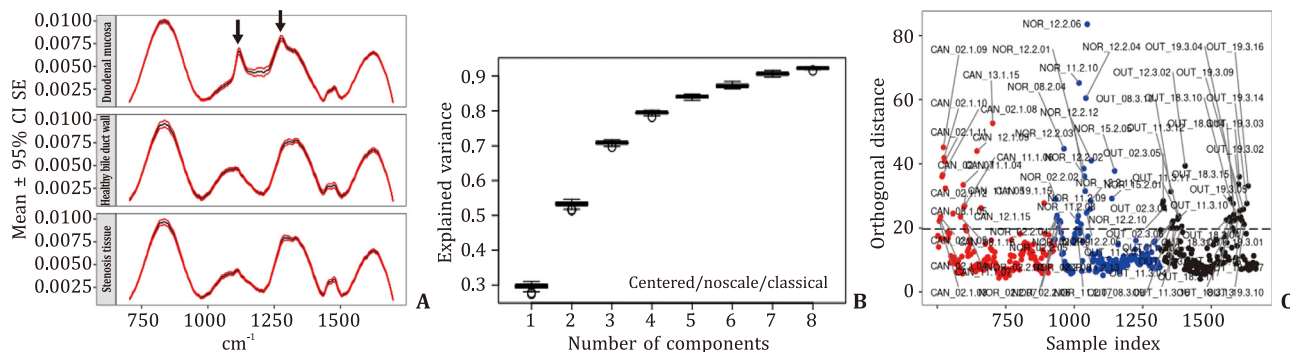


**Fig. 3. A:** Processed average Raman spectra from the analysis of three sets of samples for healthy bile duct wall, stricture and duodenal mucosa. Red spectra represent mean spectrum  $\pm$  standard error (SE) at 95 % confidence interval (CI). Spectra obtained for stricture and healthy tissues were at first sight similar, and there were also visible region differences from 1000–1300  $\text{cm}^{-1}$  for duodenal mucosa, marked by arrows and grey background for a better comparison across various types of samples. **B:** Analysis of the number of components for principal component analysis. The number of components for further processing was selected based on the percentage of total variance captured by principal components. The captured total variance did not considerably increase when more than eight components were selected. **C:** Analysis of orthogonal distance for concrete measurements. The analysis of the orthogonal distance uncovered a moderate spectral difference among some types of samples, which could be caused by a biological variance, changing environment around the Raman probe, differences in angles between the measured tissue and the probe, etc.

most cases covered the majority of the spectral variance. Influence of the present fluorescence spectral background was minimized by a subtraction of polynomial functions ( $n = 5$ ). Spectra were then normalized using a probabilistic quotient normalization that offers reliable performance in the processing of spectral data, including data obtained using Raman spectroscopy [31]. Spectral noise was treated using the well accepted Savitsky-Golay algorithm. Data were subjected to a statistical evaluation without a derivation step, as it did not lead to considerable improvements in the subsequent analysis (data not shown). The overview of the processed spectral datasets can be seen in Fig. 3A for all three measured tissue types, namely healthy bile duct wall, stricture tissue and duodenal mucosa. Fig. 3A shows the average spectra together with lower and upper 5 % ranges. Spectra obtained for stricture and healthy tissues were at first sight similar, and there were also visible region differences from 1000–1300  $\text{cm}^{-1}$  for duodenal mucosa, marked by arrows and grey background for a better comparison across various types of samples. Next, we performed a principal component analysis (PCA). The PCA was performed to evaluate i) if there are any outliers in the measured datasets, ii) understand the data, iii) determine the minimum number of components necessary to describe a data set and, in effect, remove noise and remaining redundant information. The number of components for further processing was selected based on the percentage of total variance captured by principal components (Fig. 3B). The captured total variance did not considerably increase when more than eight components were selected. We thus performed further processing with eight components. The analysis of the orthogonal distance (Fig. 3C) uncovered a moderate spectral difference among some types of samples, which could be caused by a biological variance, changing environment around the Raman probe, differences in angles between the measured tissue and the probe, etc. We decided to continue working with all data in this preliminary scenario. The attained heat map (Fig. 4A) indicated a considerable spectral difference between the resulting data for duodenal mucosa (labelled as “OUT”) and internal parts of the bile duct (labelled as “NOR” for healthy tissue and “CAN” for stenosis), which was in agreement with previously shown average spectral data. This phenomenon was further projected in Fig. 4B, which showed that a considerable number of points obtained for duodenal mucosa did not overlap with points obtained for the remaining two sample types. Unfortunately, spectral data of cancerous and healthy tissues overlapped considerably, which could indicate probable issues for their further discrimination. Finally, Fig. 4C shows the results of the discriminant cluster analysis performed on the data resulting from the

PCA, which means data with decreased dimensionality [32]. Cluster analysis, in this case based on the partial least squares approach (partial least squares discriminant analysis, PLS-DA in particular), can be considered as an automated search for groups of related observations in each dataset. The PLS-DA method allows the PLS algorithm to be used for classification as well. It performs similarly to PLS. The response vector  $y$  contains categorical vectors rather than continuous vectors. PLS-DA performs well over large data-frames and is not influenced by collinearity [33,34]. There are two key issues to be resolved: i) selection of the clustering method, and ii) determination of the number of clusters. In the mixture modelling approach applied here, both can be covered by a model selection. In our case, the model was selected based on the Bayesian approach, where the VVV (varying volume, varying shape, varying orientation – ellipsoidal covariance) model gave the best performance. The attained results indicate a possibility for discrimination among all three sample types. However, many data clusters are overlapping, and further spectral analyses are needed to perform discrimination with adequate selectivity and sensitivity.

Shim et al. first performed Raman spectroscopy of the gastrointestinal tract in 2000 [35]. They used a fiber probe with a 785 nm laser. The probe consisted of a central delivery fiber with a core diameter of 400  $\mu\text{m}$  surrounded by seven collection fibers with a core diameter of 300  $\mu\text{m}$  that could pass through the accessory channel of the endoscope [35]. Bergholt et al. demonstrated that the Raman endoscopy technique has potential for real-time diagnosis of oesophageal carcinoma [25]. Huang et al. showed the possibility of Raman spectroscopy for non-invasive endoscopic diagnosis of cancerous lesions in the stomach [20]. There have also been other studies successfully using Raman spectroscopy in the discrimination of physiological, premalignant and malignant gastric tissue [24,36,37]. Noothalapati et al. particularly reviewed several studies with a potential use of Raman spectroscopy in colorectal cancer screening [38]. Raman spectroscopy has been suggested as a viable alternative due to its potential as a rapid non-invasive diagnostic tool [38]. However, CC diagnosis using spectra techniques has thus far been overlooked.

The current standard for diagnosing biliary stricture relies on histological or cytological examination of endoscopic specimens by the pathologist. However, early malignant lesions can be difficult to identify due to limited sensitivity of current diagnostic modalities [2].

The main aim of our study was to perform Raman spectroscopy for the diagnosis of biliary stricture during ERCP. Molecular changes of biliary stricture, localized by previous imaging meth-

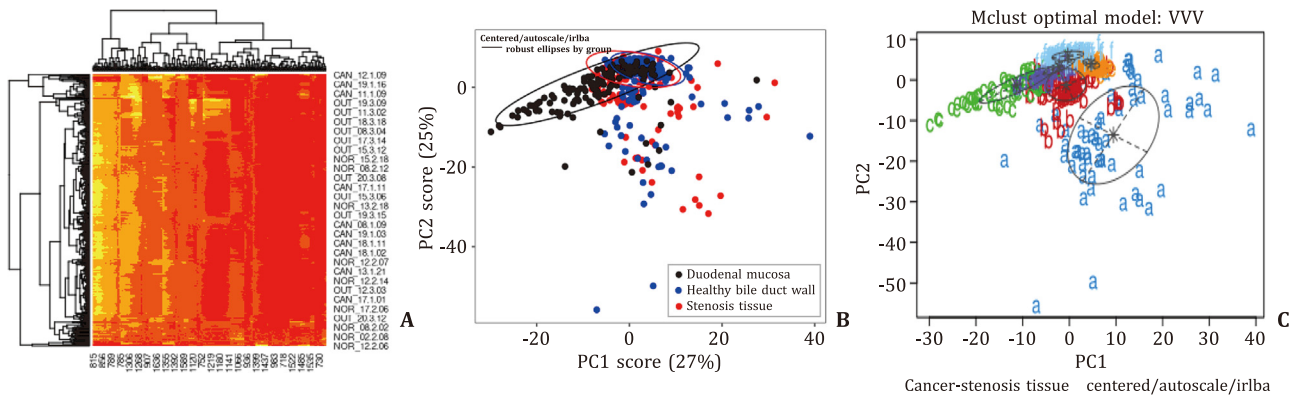


**Fig. 4.** **A:** Heat map and dendrograms for all sample types, namely healthy wall (label NOR), stenosis (label CAN) and duodenal mucosa (label OUT). The attained heat map indicated a considerable spectral difference between the resulting data for duodenal mucosa and internal parts of the bile duct (healthy tissue and stenosis), which was in agreement with previously shown average spectral data. This phenomenon was further projected in Fig. 4B. **B:** Results of the principal component analysis (PCA) for principal components 1 and 2, with Raman spectra of healthy bile duct (blue), stenosis tissue (red), and duodenal mucosa (black) of the measured sections. Spectral data obtained from tissue analysis of stenosis and healthy bile duct overlapped significantly, which could indicate probable issues for their further discrimination. However, there was a considerable number of points obtained for duodenal mucosa not overlapping with points obtained for the remaining two sample types, which indicated the possibility of distinguishing these samples. **C:** Results of the cluster analysis performed on PCA data using the VVV (varying volume, varying shape, varying orientation) model. Figure shows the results of the discriminant cluster analysis performed on the data resulting from the PCA analysis, which means data with decreased dimensionality.

ods, were assessed in real time. These identified intra-tissue Raman biomolecular signals could be advantageously used to guide the endoscopist to biopsy suspected biliary stricture, as well as for their staging, given that while imaging methods are limited to imaging a visible stricture, Raman spectroscopy can diagnose malignant tumor tissue even in places where there is no visible stricture. The unrivalled advantage of the Raman spectroscopy technique stems from its capability to uncover specific information about backbone structures of proteins, lipids and nucleic acid assemblies in cells and tissue [33,39].

To date, Raman spectroscopy combined with gastrointestinal endoscopic evaluation tissue has mostly been focused on evaluating the oesophagus, gastric and colon tissue. The clinical significance of Raman spectroscopy is underestimated due to standardization of the instrument, data analysis and operative procedures. The combined technique of Raman spectroscopy and endoscopy identifies tissue areas for sampling and enables rapid non-invasive diagnosis based on molecular information [38]. The Raman spectroscopy measurement itself, moreover, has no cost. However, Raman spectroscopy combined with endoscopy offers unique opportunities to develop a low-cost non-invasive method that is suitable for large scale screening of malignant lesions in the oesophagus, stomach and colon.

For the first-time, we investigated biliary stricture with Raman spectroscopy, physiological tissue of bile ducts and duodenal mucosa during ERCP and explore the potential of translating Raman biomolecular spectral differences between normal and malignant bile tissue for realizing endoscopic diagnosis of cancerous lesions in the bile duct. Unlike endoscopy of the oesophagus, stomach and colon, endoscopy of the bile ducts, cholangioscopy, is an expensive method and is difficult to perform.

Our results indicated a possibility to discriminate between the spectra of duodenal mucosa from spectra of healthy bile ducts and stricture. However, discrimination of stricture from the healthy bile duct wall still presents a considerable challenge. This unique endoscopic approach based on real-time Raman spectroscopy has the potential to open a new avenue for objective diagnosis of CC *in vivo* at the molecular level.

The introduction of the spectroscopy probe into the bile ducts was sometimes challenging due to the limited flexibility of the probe, obturation of Vater's papilla by the tumor mass, anatomical conditions and the resulting difficult cannulation of the bile

ducts with a metal sheath. In one case (distal extrahepatic CC) the introduction was successful, the tumorous tissue filled the lumen of the bile duct, so we did not measure physiological tissue. In another five cases of failure (1 CC, 3 ampullary tumors, 1 physiological finding on the bile duct), the introduction was limited by individual anatomical conditions, mainly the angle of separation of the bile ducts, peripapillary diverticula and the size of the lumen. Importantly, we did not notice any increased occurrence of complications during the procedure compared to conventional ERCP. None of the patients developed acute post-ERCP pancreatitis or any other complication.

We measured spectra for biliary stenosis, physiological bile duct tissue and duodenal mucosa. The spectra of duodenal mucosa were in many cases visually different from those determined for biliary tissue, confirming the promising potential of Raman endoscopy for detection of neoplastic lesions in the bile duct during ERCP examination. Moreover, the results attained from the performed mathematical analysis further support this potential. However, the performed statistical analysis thus far did not uncover a significant Raman spectral difference between tumor biliary stenosis and physiological biliary tissue. The reason is probably a complex mix of interfering effects, including a lower number of performed measurements or high levels of present fluorescence (Fig. 3A). This can be caused by a presence of blood and bile in the measured points of interest, as both also have high levels of autofluorescence in the range of the applied excitation source operating at 785 nm. Possible solutions to this challenge include increasing the number of analyzed samples and introducing more capable statistical models.

Raman spectroscopy in endoscopy has some limitations. The detection of scattering of photons in tissues typically requires physical contact between the optical probe and the target tissue and can characterize only a small portion of a suspicious lesion [40,41]. Another limitation is autofluorescence which can be much stronger than Raman signals that can be masked by the fluorescence background [42]. It is important to mention that reproducibility can be jeopardized due to the variability in endoscopists and the pressure they apply to the contact probe against the tissue [42].

In conclusion, transpapillary Raman spectroscopy of biliary stricture is feasible. We have successfully developed a Raman endoscopic technique that can acquire spectra for biliary stricture and physiological bile duct tissue. Although duodenal and biliary Ra-

man spectroscopy patterns were different, no significant difference between CC and normal bile duct was observed. We did not have enough data to evaluate whether there are differences in the measured spectra between CC/physiological bile tissue and other types of biliary strictures. Raman spectroscopy is a promising technique for tissue diagnosis of biliary stricture. Further studies with larger number of patients and the introduction of more complex statistical methods are thus necessary to differentiate between physiological and malignant biliary tissue.

## Acknowledgments

This study is dedicated to the memory of Mgr. Vlastimil Mašek, PhD.

## CRediT authorship contribution statement

**Peter Slodička:** Conceptualization, Data curation, Formal analysis, Investigation, Project administration, Writing – original draft. **Přemysl Falt:** Conceptualization, Data curation, Methodology, Writing – review & editing. **Václav Ranc:** Investigation, Methodology, Resources, Software, Writing – original draft, Writing – review & editing. **Vincent Dansou Zoundjiekpon:** Data curation, Writing – original draft. **Ondřej Urban:** Conceptualization, Data curation, Funding acquisition, Supervision, Visualization, Writing – review & editing.

## Funding

This study was supported by the grant from MH CZ–DRO (FNOL, 00098892).

## Ethical approval

The study was approved by the Ethics Committee of the University Hospital and Faculty of Medicine of Palacky University in Olomouc. Written informed consent was obtained from all participants.

## Competing interest

No benefits in any form have been received or will be received from a commercial party related directly or indirectly to the subject of this article.

## References

- [1] Tummala P, Munigala S, Eloubeidi MA, Agarwal B. Patients with obstructive jaundice and biliary stricture ± mass lesion on imaging: prevalence of malignancy and potential role of EUS-FNA. *J Clin Gastroenterol* 2013;47:532–537.
- [2] Singh A, Gelrud A, Agarwal B. Biliary strictures: diagnostic considerations and approach. *Gastroenterol Rep (Oxf)* 2015;3:22–31.
- [3] Bergquist A, von Seth E. Epidemiology of cholangiocarcinoma. *Best Pract Res Clin Gastroenterol* 2015;29:221–232.
- [4] Oliveira IS, Kilcoyne A, Everett JM, Mino-Kenudson M, Harisinghani MG, Ganesan K. Cholangiocarcinoma: classification, diagnosis, staging, imaging features, and management. *Abdom Radiol (NY)* 2017;42:1637–1649.
- [5] Blechacz B, Komuta M, Roskams T, Gores GJ. Clinical diagnosis and staging of cholangiocarcinoma. *Nat Rev Gastroenterol Hepatol* 2011;8:512–522.
- [6] Esnaola NF, Meyer JE, Karachristos A, Maranki JL, Camp ER, Denlinger CS. Evaluation and management of intrahepatic and extrahepatic cholangiocarcinoma. *Cancer* 2016;122:1349–1369.
- [7] Kendall T, Verheij J, Gaudio E, Evert M, Guido M, Goepfert B, et al. Anatomical, histomorphological and molecular classification of cholangiocarcinoma. *Liver Int* 2019;39(Suppl 1):7–18.
- [8] Ilyas SI, Khan SA, Hallemeier CL, Kelley RK, Gores GJ. Cholangiocarcinoma - evolving concepts and therapeutic strategies. *Nat Rev Clin Oncol* 2018;15:95–111.
- [9] Urban O, Vanek P, Zoundjiekpon V, Falt P. Endoscopic perspective in cholangiocarcinoma diagnostic process. *Gastroenterol Res Pract* 2019;2019:9704870.
- [10] Doherty B, Nambudiri VE, Palmer WC. Update on the diagnosis and treatment of cholangiocarcinoma. *Curr Gastroenterol Rep* 2017;19(2).

- [11] Ruys AT, van Beem BE, Engelbrecht MR, Bipat S, Stoker J, Van Gulik TM. Radiological staging in patients with hilar cholangiocarcinoma: a systematic review and meta-analysis. *Br J Radiol* 2012;85:1255–1262.
- [12] Zhang H, Zhu J, Ke F, Weng M, Wu X, Li M, et al. Radiological imaging for assessing the respectability of hilar cholangiocarcinoma: a systematic review and meta-analysis. *Biomed Res Int* 2015;2015:497942.
- [13] Razumilava N, Gores GJ. Classification, diagnosis, and management of cholangiocarcinoma. *Clin Gastroenterol Hepatol* 2013;11:13–21 e1; quiz e3–4.
- [14] Brooks C, Gausman V, Kokoy-Mondragon C, Munot K, Amin SP, Desai A, et al. Role of fluorescent in situ hybridization, cholangioscopic biopsies, and EUS-FNA in the evaluation of biliary strictures. *Dig Dis Sci* 2018;63:636–644.
- [15] Liew ZH, Loh TJ, Lim TKH, Lim TH, Khor CJL, Mesenas SJ, et al. Role of fluorescence in situ hybridization in diagnosing cholangiocarcinoma in indeterminate biliary strictures. *J Gastroenterol Hepatol* 2018;33:315–319.
- [16] Barr Fritcher EG, Voss JS, Brankley SM, Campion MB, Jenkins SM, Keeney ME, et al. An optimized set of fluorescence in situ hybridization probes for detection of pancreatobiliary tract cancer in cytology brush samples. *Gastroenterology* 2015;149:1813–1824 e1.
- [17] Urban O, Evinová E, Fojtík P, Loveček M, Kliment M, Zoundjiekpon V, et al. Digital cholangioscopy: the diagnostic yield and impact on management of patients with biliary stricture. *Scand J Gastroenterol* 2018;53:1364–1367.
- [18] Park J, Kim MH, Kim KP, Park DH, Moon SH, Song TJ, et al. Natural history and prognostic factors of advanced cholangiocarcinoma without surgery, chemotherapy, or radiotherapy: a large-scale observational study. *Gut Liver* 2009;3:298–305.
- [19] Sharma N, Takeshita N, Ho KY. Raman spectroscopy for the endoscopic diagnosis of esophageal, gastric, and colonic diseases. *Clin Endosc* 2016;49:404–407.
- [20] Huang Z, Teh SK, Zheng W, Lin K, Ho KY, Teh M, et al. In vivo detection of epithelial neoplasia in the stomach using image-guided Raman endoscopy. *Biosens Bioelectron* 2010;26:383–389.
- [21] Huang Z, Teh SK, Zheng W, Mo J, Lin K, Shao X, et al. Integrated Raman spectroscopy and trimodal wide-field imaging techniques for real-time in vivo tissue Raman measurements at endoscopy. *Opt Lett* 2009;34:758–760.
- [22] Bergholt MS, Lin K, Wang J, Zheng W, Xu H, Huang Q, et al. Simultaneous fingerprint and high-wavenumber fiber-optic Raman spectroscopy enhances real-time in vivo diagnosis of adenomatous polyps during colonoscopy. *J Biophotonics* 2016;9:333–342.
- [23] Teh JL, Shabbir A, Yuen S, So JB. Recent advances in diagnostic upper endoscopy. *World J Gastroenterol* 2020;26:433–447.
- [24] Bergholt MS, Zheng W, Lin K, Ho KY, Teh M, Yeoh KG, et al. Raman endoscopy for in vivo differentiation between benign and malignant ulcers in the stomach. *Analyst* 2010;135:3162–3168.
- [25] Bergholt MS, Zheng W, Lin K, Ho KY, Teh M, Yeoh KG, et al. In vivo diagnosis of esophageal cancer using image-guided Raman endoscopy and biomolecular modeling. *Technol Cancer Res Treat* 2011;10:103–112.
- [26] Bergholt MS, Zheng W, Ho KY, Teh M, Yeoh KG, So JB, et al. Fiber-optic Raman spectroscopy probes gastric carcinogenesis in vivo at endoscopy. *J Biophotonics* 2013;6:49–59.
- [27] Teh SK, Zheng W, Ho KY, Teh M, Yeoh KG, Huang Z. Near-infrared Raman spectroscopy for early diagnosis and typing of adenocarcinoma in the stomach. *Br J Surg* 2010;97:550–557.
- [28] Stomp-Agenant M, van Dijk T, R Onur A, Grimbergen M, van Melick H, Jonges T, et al. In vivo Raman spectroscopy for bladder cancer detection using a superficial Raman probe compared to a nonsuperficial Raman probe. *J Biophotonics* 2022;15:e202100354.
- [29] Ke ZY, Ning YJ, Jiang ZF, Zhu YY, Guo J, Fan XY, et al. The efficacy of Raman spectroscopy in lung cancer diagnosis: the first diagnostic meta-analysis. *Lasers Med Sci* 2022;37:425–434.
- [30] Chen C, Hao J, Hao X, Xu W, Xiao C, Zhang J, et al. The accuracy of Raman spectroscopy in the diagnosis of lung cancer: a systematic review and meta-analysis. *Transl Cancer Res* 2021;10:3680–3693.
- [31] Dieterle F, Ross A, Schlotterbeck G, Senn H. Probabilistic quotient normalization as robust method to account for dilution of complex biological mixtures. Application in 1H NMR metabolomics. *Anal Chem* 2006;78:4281–4290.
- [32] Fraley C, Raftery AE. Model-based clustering, discriminant analysis and density estimation. *J Am Stat Assoc* 2002;97:611–631.
- [33] Pérez-Enciso M, Tenenhaus M. Prediction of clinical outcome with microarray data: a partial least squares discriminant analysis (PLS-DA) approach. *Hum Genet* 2003;112:581–592.
- [34] Nguyen DV, Rocke DM. Tumor classification by partial least squares using microarray gene expression data. *Bioinformatics* 2002;18:39–50.
- [35] Shim MG, Song LM, Marcon NE, Wilson BC. In vivo near-infrared Raman spectroscopy: demonstration of feasibility during clinical gastrointestinal endoscopy. *Photochem Photobiol* 2000;72:146–150.
- [36] Wang J, Lin K, Zheng W, Ho KY, Teh M, Yeoh KG, et al. Fiber-optic Raman spectroscopy for in vivo diagnosis of gastric dysplasia. *Faraday Discuss* 2016;187:377–392.
- [37] Luo S, Chen C, Mao H, Jin S. Discrimination of premalignant lesions and cancer tissues from normal gastric tissues using Raman spectroscopy. *J Biomed Opt* 2013;18:067004.
- [38] Noothalapati H, Iwasaki K, Yamamoto T. Non-invasive diagnosis of colorectal cancer by Raman spectroscopy: recent developments in liquid biopsy and endoscopy approaches. *Spectrochim Acta A Mol Biomol Spectrosc* 2021;258:119818.

- [39] Bergholt MS, Zheng W, Ho KY, Teh M, Yeoh KG, Yan So JB, et al. Fiberoptic confocal raman spectroscopy for real-time in vivo diagnosis of dysplasia in Barrett's esophagus. *Gastroenterology* 2014;146:27–32.
- [40] Garai E, Sensarn S, Zavaleta CL, Loewke NO, Rogalla S, Mandella MJ, et al. A real-time clinical endoscopic system for intraluminal, multiplexed imaging of surface-enhanced Raman scattering nanoparticles. *PLoS One* 2015;10:e0123185.
- [41] Jeong S, Kim YI, Kang H, Kim G, Cha MG, Chang H, et al. Fluorescence-Raman dual modal endoscopic system for multiplexed molecular diagnostics. *Sci Rep* 2015;5:9455.
- [42] Zavaleta CL, Garai E, Liu JT, Sensarn S, Mandella MJ, Van de Sompel D, et al. A Raman-based endoscopic strategy for multiplexed molecular imaging. *Proc Natl Acad Sci U S A* 2013;110:E2288–E2297.

Received 22 May 2024  
Accepted 8 November 2024  
Available online xxx